Optik - International Journal for Light and Electron Optics 266 (2022) 169519

Contents lists available at ScienceDirect

Optik

journal homepage: www.elsevier.com/locate/ijleo

Numerical analysis of the behavioral response of pump-modulated linear and ring erbium-doped fiber lasers

Nneka Obianuju Onubogu [a], Chang Hong Pua [a,*], Abd-Rahman Faidz [a], William C. Rose [b]

[a] Lee Kong Chian Faculty of Engineering and Science, Universiti Tunku Abdul Rahman, Jalan Sungai Long, Bandar Sungai Long, 43000 Kajang, Selangor, Malaysia
[b] Department of Kinesiology and Applied Physiology, University of Delaware, Newark, DE 19716, USA

ARTICLE INFO

Keywords:
Erbium-doped fiber laser
Rate equations
Pump modulation
Bifurcation
Chaos

ABSTRACT

Objective: The behavioral response of an erbium-doped fiber laser having two different configurations (linear cavity and ring cavity) and subjected to pump modulation is analyzed numerically. These same laser configurations with the same initial conditions have previously been studied experimentally.
Methodology: For the numerical analysis, a modified laser model based on the rate equations of a three-level class B laser which is quite similar to that of a non-linear oscillator is presented.
Results: The numerical model generates all the linear and non-linear spectral features observed during the experimental analysis. The experimental and numerical bifurcation, time domain and frequency domain diagrams match reasonably well. The dynamic behavior of the EDFRL is numerically analyzed at low modulation frequencies (below 7 kHz) when the resonance frequency ranges from 2 kHz to 10 kHz. The results for the descending chirp of the EDRFL under certain pump modulation conditions showed a new strange dynamic behavior requiring further studies.
Significance: The EDFRL can be used for sensing purposes in locations with high background noise as it is sensitive even at low frequencies irrespective of the noise. Numerical analysis is a fast and reliable way to obtain remarkable information on the spectral behavior of the EDFL.

1. Introduction

The merits of erbium-doped fiber lasers (EDFLs) have made them popular for so many years and counting in the areas of secure optical communication, medicine, sensing, LIDAR technology, etc. [1–10]. These merits include their immunity to electro-magnetic interference, narrow line-width, one-mode operation, slow relaxation times, long interaction length of the laser pumped light with the active erbium ions, high amplification or gain, low noise, great sensitivity to external perturbations leading to a series of dynamic behaviors, etc., [7]. More so, EDFLs are very compact in size and affordable which makes them applicable in hand-held detectors [11]. Hence, it is of great interest to many researchers to study the dynamic features of the EDFL especially under modulation owing to its many developing prospective applications.

* Corresponding author.
E-mail addresses: nneka.onubogu@1utar.my (N.O. Onubogu), puach@utar.edu.my (C.H. Pua), faidzar@utar.edu.my (A.-R. Faidz), rosewc@udel.edu (W.C. Rose).

https://doi.org/10.1016/j.ijleo.2022.169519
Received 19 April 2022; Received in revised form 1 June 2022; Accepted 16 June 2022
Available online 20 June 2022

Many studies have been carried out on the experimental and theoretical pump modulation of EDFLs with linear and ring resonators where the EDFLs exhibited self-pulsation, linear and non-linear (chaotic) behavior and optical bi-stability [6,12–28]. Nevertheless, this type of study is endless as new features are observed with different EDFL configurations. Most of the existing studies developed a simple or complex theoretical model based on their EDFL configuration which described their experimental results well. Our laser configurations are different from those studied by other authors and are quite simple and affordable. Therefore, the existing theoretical models cannot accurately describe our EDFLs. The model of Pisarchik et al. [12] is closely related to our laser configurations, hence modification and improvement have been made based on their existing model in order to get a model that describes our laser and produces simulation results that match our experimental results reasonably well. In our modification, we consider the resonance frequency of the EDFL at a particular time since the EDFL is a resonator and can have different resonance frequencies at different times. This is important for characterization of the EDFL's sensitivity to acoustic waves detection. Pisarchik et al.'s model only considered the relaxation oscillation frequency of the EDFL and provided simulation results for two cases only: when the modulation frequency is higher and lower than the relaxation oscillation frequency respectively. Also, in the modified code, the driving function is a chirp, and so the simulation runs once over a range of frequencies; where the initial and final modulation frequencies and the duration are specified in the code. This gives more accurate results. In comparison with the original model where the self-pulsating behavior does not appear, our model shows the self-pulsing behavior of the EDFL when there is no modulation as the saturable absorber phenomenon is accounted for.

Previously, we reported on the experimental pump-modulation of our linear and ring EDFLs and presented in detail the linear and non-linear behaviors and other features observed [25–27]. In this study, we present the numerical simulation of both EDFLs subjected to pump-modulation using parameters similar to those used in our experiments. Numerical bifurcation diagrams obtained agree reasonably well with our experimental bifurcation diagrams. Our model is able to envisage the linear and non-linear (chaotic) behavior including optical-bistability exhibited under certain pump modulation input conditions. Based on the behaviors observed, the EDFL has excellent potential to be used as a sensor, as it revealed high sensitivity at its resonance frequency.

The next four sections of this paper cover an explanation of the configuration and experimental set-ups of the EDFLs (Section 2); theoretical model of the erbium-doped fiber laser (linear and ring) where we present the modified laser model and the normalized equations for the two laser configurations (Section 3); the numerical pump-modulation results for both laser configurations to match with our experimental results where we also explain the dynamics of our erbium-doped fiber ring laser at low modulation frequencies (MF) under various resonance frequencies (RF) (Section 4) and finally the conclusion is given in Section 5.

2. Configuration and experimental set-up of the EDFLs (linear and ring)

With reference to [26,27] and [25], brief explanations of the configuration or experimental set-ups of the erbium doped fiber linear laser (EDFLL) and the erbium-doped fiber ring laser (EDFRL) are given.

2.1. Configuration and experimental set-up of the EDFLL

The EDFLL resonator comprises a 3 m 980/1550 nm high performance wavelength division multiplexer (WDM) coupled to a 3 m length erbium doped fiber (EDF) as an active medium having 8 μm diameter core and 125 μm diameter clad. A 3 m length single mode fiber (SMF), is coupled to the EDF acting as a sensing arm to sense acoustic waves and vibration. The SMF is finally coupled to 1550 nm single side fiber Bragg grating (FBG), with a center wavelength of 1550 nm ± 0.3 nm, and > 99% reflectivity. The entire laser cavity length is about 10 m. When the EDFLL is subjected to pump modulation, a manual function generator and digital oscilloscope are connected to the single wavelength 980 nm diode laser pump (Gooch & Housego EM595) with a sinusoidal modulation waveform to modulate the frequency and voltage of the pumped light. The diode laser pump, with a maximum pump power of 245 mW propels 980 nm photons into the WDM which couples the photons into the EDF. The photons are absorbed by the erbium ions in the EDF and

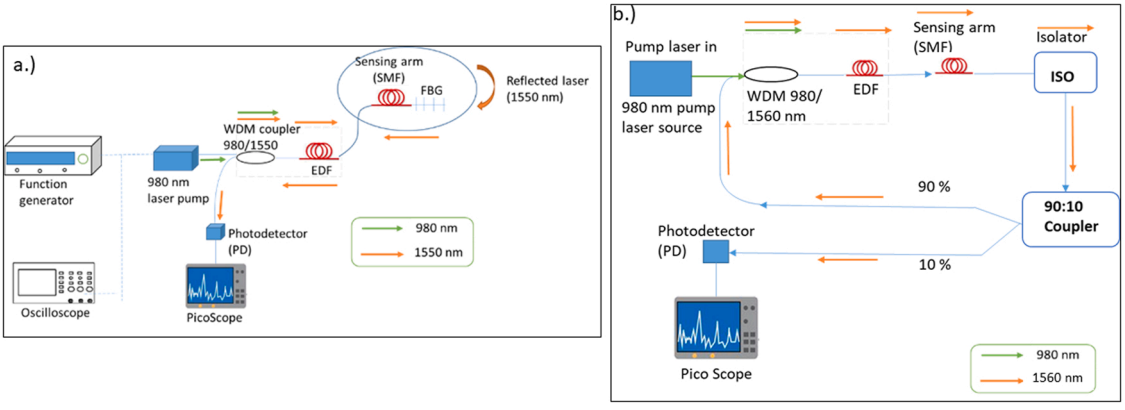

Fig. 1. Experimental configuration of the (a) EDFLL [26,27]; (b) EDFRL [25].

1520–1560 nm wavelength photons are spontaneously emitted. The FBG then reflects only 1550 nm wavelength photons back to the laser cavity. The erbium ions are then stimulated by the reflected 1550 nm photons to release more photons at 1550 nm. A photodetector (THORLABS-DET08CFC/M) converts the optical output to electrical output and sends it to an oscilloscope (PicoScope 6 (3000 series)) used to monitor the spectrum of the laser output. The configuration of the pump-modulated EDFLL is shown in Fig. 1(a) where the green and orange arrows signify the optical paths of 980 nm and 1550 nm wavelength photons.

2.2. Configuration and experimental set-up of the EDFRL

The EDFRL resonator comprises a single wavelength 980 nm pump laser that pumps photons which are launched into the EDF through a WDM. The specifications of the WDM and EDF are as mentioned in Section 2.1. The frequency and voltage of the 980 nm pump laser are modulated with a manual function generator (GWINSTEK GFG-8020 H). From the EDF, the photons move to a 3 m length SMF called the sensing arm which is coupled to a 1550 nm isolator to ensure the unidirectional transmission of photons in the laser resonator. The isolator is coupled to a 90/10 coupler which taps 10% of the intra-cavity laser power and directs it to the photodetector to monitor the spectral response of the laser via an oscilloscope. 90% of the laser output is fed back into the ring cavity and the cycle continues. No polarizer is used in this set-up. The length of the EDFRLs lasing cavity is about 13 m. The experimental configuration of the EDFRL is presented in Fig. 1(b).

3. Theoretical model of the EDFLL and EDFRL

Pump modulation has been carried out experimentally as shown in our previous publications [25–27]. Our laser system is classified as a three-level class B laser system where its polarization decay rate is of the order 10^{11} s^{-1}; its population decay rate from the lasing level is of the order 10^{2} s^{-1} and the decay rate of its lasing field is of the order of magnitude 10^{7} s^{-1}. This entails that the polarization decay rate of our laser system is considerably higher than that of its population inversion and lasing field [29], hence the polarization variable is negligible [20,30].

EDFLs are generally three-level laser systems where $E_1 < E_2 < E_3$ and $N_2 > N_1 > N_3$. E as shown in Fig. 2 signifies the energy levels while N signifies the number of electrons in each energy level. When a pump laser of 980 nm wavelength is turned on, photons are emitted and are absorbed by the electrons at E_1. When the electrons at E_1 gains sufficient energy, they get excited and transit to higher energy level E_3. The lifetime of electrons at level E_3 is short, hence after a very short period, the electrons instantaneously fall to the meta-stable level E_2 by non-radiative emission (Θ_{32}). At E_2, the life time of the electrons is longer than that of E_3 causing a large amount of electrons to accumulate at E_2 compared to E_3 and E_1. This is called population inversion which leads to lasing. After completion of the lifetime of electrons at E_2, they drop to E_1 releasing a photon by spontaneous emission (Θ_{21}). This photon reacts with the electrons at E_2, compelling another electron to drop to E_1 releasing two photons via stimulated emission. The process continues and numerous photons are emitted as long as the laser medium is being pumped.

The model used to obtain similar experimental results in Onubogu et al. [27] for linear laser and Onubogu and Pua [25] for ring laser, is a modified version of Pisarchik et al.'s model [12] and is based on the two rate equations of a three-level laser for intra-cavity laser power (L_p) and population inversion ($\overline{N_2}$). L_p is measured in inverse seconds (s^{-1}) and is the total power of the waves contra-propagating within the laser resonator (12, 20, 29). $\overline{N_2}$ is a dimensionless variable where $0 \leq \overline{N_2} \leq 1$ and it refers to the average population of the upper level (total concentration of the erbium ions at N_2) along the length of the pumped active fiber. Fig. 2 shows the energy-level illustration of our model. The rate equations are shown below:

$$\frac{dL_p}{dt} = S_e(t) + 4LL_p\frac{1}{2t_R}\{Q_0Q_w[\overline{N_2}(\Sigma_1 - \Sigma_2) - 1] - \alpha_{th}\} \tag{1}$$

$$\frac{d\overline{N_2}}{dt} = P_{pump}(t) - (\Theta_{12}Q_wL_p)\frac{1}{\pi r_0^2}(\overline{N_2}\Sigma_1 - 1) - \frac{\overline{N_2}}{\tau_2} \tag{2}$$

The definition of all the variables in Eqs. (1) and (2) above and other parameters used in the numerical analysis are in Table 1. Eqs. (1) and (2) describe the dynamic behavior of the EDFL when there is zero external modulation. To trigger the non-linear dynamic

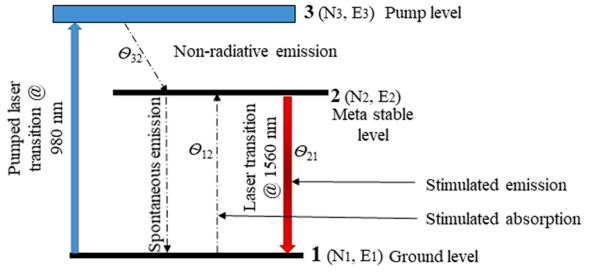

Fig. 2. Energy-level diagram of the Erbium ions in the EDFL system (Note: Laser transition is @ 1550 nm for linear laser and @ 1560 nm for ring laser).

Table 1
Variables, parameters, and their values, used in the numerical analysis. Variables and parameters without units are non-dimensional.

Variable	Description
$\overline{N_2}$	$\overline{N_2} = (\frac{1}{n_O L}) \int_O^L N_2(z)dz$ The average population of the upper level along the length of the pumped active fiber.
L_p (s^{-1})	Total powers of the waves contra-propagating inside the laser resonator.
N_1	Population of ground level 1
N_2	Population of upper /meta -stable level 2
S_e	$S_e = \frac{Q_o \lambda_g^2 L \overline{N_2}}{\tau_2 t_R \Theta_{12}} \frac{r_0^2 10^{-3}}{4(\pi r_f)^2}$ The spontaneous emission into the fundamental laser mode.
PP	Pump power at fiber entrance: $PP = PP_1^0[1 + A_m \sin 2\pi F_m t]$
P_{pump}	Pump power: $P_{pump} = \frac{PP[1 - e^{[-L.Q_p + LQ_p N_i]}]}{\pi r_o^2 L N_0}$
R_1	$R_1 = PP \frac{\tau_2 Q_w \mho_2}{\pi r_o^2 L N_0}$ where $\frac{\tau_2 Q_w \mho_2}{\pi r_o^2 L N_0} = 4.819 \times 10^{-18}$

Parameter	**Value**	**Description**
n_0	1.45	The refractive index of the core of a "cold" EDF
L (cm)	300	For linear laser: The length of the EDF
	1300	For ring laser: The length of the resonator which includes the length of the EDF (300 cm)
t_R (ns)	31	$t_R = \frac{2n_0(L + l_{FBG})}{c}$ {for linear cavity laser}
	10	$t_R = \frac{L}{c}$ {for ring cavity laser} This is the time taken for the photon to travel inside the resonator/cavity per cycle.
l_{FBG} (cm)	20	Full length of the FBG coupler end inside the resonator.
c (cm/s)	29.979×10^9	Speed at which photons travel in the resonator.
Q_0 (cm^{-1})	0.0534	$Q_0 = N_o \Theta_{12}$ The co-efficient that describes the small signal-absorption or resonant-absorption properties of the EDF at the laser wavelength.
N_o (cm^{-3})	5.4×10^{19}	$N_o = N_1 + N_2$ The sum of the concentration of erbium ions in the active fiber.
$\Theta_{12} = \Theta_{21}$ (cm^2)	3×10^{-21}	Θ_{12} = Cross-section of the absorption transition from the lower /ground level 1 to meta-stable level 2. Θ_{21} = Cross-section of the return stimulated transition from meta-stable level 2 to ground level 1.
Θ_{23} (cm^2)	0.9×10^{-21}	Cross-section of the excited-state absorption (ESA) from meta-stable level 2 to upper level 3.
Q_w	0.829	$Q_w = 1\text{-}e^{[-2(r_0/r_f)]}$ This is the factor that signifies a match between the fundamental mode of the laser and the core volume of the erbium-doped active fiber.
MFD (m)	5.2×10^{-6}	Mode Field Diameter of the EDF.
r_0 (cm)	2.6×10^{-4}	The radius of the core of the EDF.
r_f (cm)	2.94×10^{-4}	$r_f = r_0(0.65 + \frac{1.619}{V^{1.5}} + \frac{2.879}{V^6})$ The radius of the EDF in fundamental mode.
V	2.30	A parameter relating the numerical aperture (NA) with the radius of the fiber core as: $V = \frac{(NA)2\pi r_0}{\lambda_g}$
NA	0.22–0.24	Numerical aperture of the fiber
λ_g (cm)	1.550×10^{-4} (linear)	The EDFL wavelength (obtained from the optical spectrum analyzer during experiments[25,26].
	1.560×10^{-4} (ring)	
ξ_1	2.0	$\xi_1 = \frac{\Theta_{12} + \Theta_{21}}{\Theta_{12}}$ The co-efficient that shows the relationship between absorption and stimulated transitions.
ξ_2	0.4	$\xi_2 = \frac{\Theta_{23}}{\Theta_{12}}$ The coefficient that shows the relationship between the cross-sections of the ESA (Θ_{23}) and ground-state absorption (Θ_{12}) at the laser wavelength.
$\mho_1$	1.6	ξ_1 - ξ_2
$\mho_2$	2.0	ξ_1
α_{th}	3.837×10^{-2}	$\alpha_{th} = \gamma_0 + (\frac{1}{2L})\ln(\frac{1}{R_{FBG}})$ {for linear cavity laser} $\alpha_{th} = \gamma_0$ {for ring cavity laser} The intra-cavity losses on the laser threshold.
γ_0	0.038	The non-resonant fiber loss.
R_{FBG}	0.8	The total reflection co-efficient of the FBG coupler.
Q_p (cm^{-1})	0.025	The co-efficient that describes the small-signal absorption or resonant-absorption properties of the EDF at the pump wavelength.
τ_2(ns)	10^7	Lifetime of erbium ions in the excited state (meta-stable state 2)

Normalized parameter values for linear and ring laser

Parameter	**Linear laser**	**Ring laser**	**Formula**
K_1	0.00603	0.00603	$\frac{\tau_2}{Q_w \mho_1}$
K_2	6.2×10^7	19.19×10^7	$2LQ_0(\frac{\tau_2}{t_R})(\frac{\mho_1}{\mho_2})$
K_3	2.03×10^7	6.26×10^7	$2L(\frac{\tau_2}{t_R})(\alpha_{th} \frac{-(\mho_1 + \mho_2)}{\mho_2 Q_w})$

(*continued on next page*)

Table 1 (*continued*)

Variable	Description		
R_1	4.819×10^{-18} *PP*	4.819×10^{-18} *PP*	$PP\,\frac{\tau_2 Q_w \mho_2}{\pi r_o^2 L N_0}$ Note: R_1 is not exactly a constant as *PP* is varied during simulation so as to set the RF. The constant here is $\frac{\tau_2 Q_w \mho_2}{\pi r_o^2 L N_0}$
R_2	1.46×10^4	4.5×10^4	$\frac{(\Theta_{12} Q_w \tau_2 \mho_2)}{\pi r_0^2 \frac{Q_o {\lambda_g}^2 L}{\tau_2 t_R \Theta_{12}} \frac{r_0^2 10^{-3}}{4(\pi r_f)^2}}$

behavior of the EDFL, another variable must be introduced via an external modulating signal. Hence the pump power at the entrance of the fiber would then be:

$$PP(t) = PP_1^0[1 + A_m \sin 2\pi F_m t] \tag{3}$$

Where *PP* is the pump power at the entrance of the fiber and PP_1^0 is the average pump power at the entrance of the fiber when there is no modulation i.e. $A_m = 0$. Parameters A_m (modulation or driving amplitude symbolized as MA in this manuscript) and F_m (modulation frequency symbolized as MF in this manuscript) can be varied in our simulation and experiment as they are pump-dependent. When there is no modulation, $PP = PP_1^0$ and PP_1^0 can be varied to estimate the relaxation oscillation frequency (which is nearly equivalent to the RF of the system) at various pump power levels. Therefore, we set the RF of our system before pump modulation is carried out by increasing or decreasing the input pump power.

With Eqs. (1) to (3) and referring to the parameters in Table 1, it is possible to theoretically analyze the behavior of the EDFLL and EDFRL subjected to pump-modulation by obtaining the time and frequency domains and the bifurcation diagrams as well. For theoretical analysis to be carried out swiftly, Eqs. (1) and (2) can be simplified in the following way:

In Eq. (1),

$$S_e(t) = \frac{Q_o {\lambda_g}^2 L \overline{N_2}(t)}{\tau_2 t_R \Theta_{12}} \frac{r_0^2 10^{-3}}{4(\pi r_f)^2} \tag{4}$$

In Eq. (2),

$$P_{pump}(t) = \frac{PP[1 - e^{[-LQ_p + LQ_p \overline{N_2}(t)]}]}{\pi r_o^2 L N_0} \tag{5}$$

Eq. (4) can be written as: $S_e(t) = q_1 \overline{N_2}(t)$; given that $q_1 = \frac{Q_o {\lambda_g}^2 L}{\tau_2 t_R \Theta_{12}} \frac{r_0^2 10^{-3}}{4(\pi r_f)^2}$.

Eq. (5) can be written as: $P_{pump}(t) = PP(t) q_2 [1 - e^{[-q_3(1-\overline{N_2}(t))]}]$; given that $q_2 = \frac{1}{\pi r_o^2 L N_0}$ and $q_3 = LQ_p$.

Assuming that $\xi_1 - \xi_2$ in Eq. (1) is equal to $\mho_1$; and $\xi_1 = \mho_2$ in Eq. (2); then:

Eq. (1) can be re-written as:

$$\frac{dL_p}{dt} = q_1 \overline{N_2}(t) + 4LL_p \frac{1}{2t_R} \{Q_0 Q_w [\overline{N_2}(\mho_1) - 1] - \alpha_{th}\} \tag{6}$$

Eq. (2) can be re-written as:

$$\frac{d\overline{N_2}}{dt} = PP(t) q_2 [1 - e^{[-q_3(1-\overline{N_2}(t))]}] - (\Theta_{12} Q_w L_p) \frac{1}{\pi r_0^2} (\overline{N_2} \mho_2 - 1) - \frac{\overline{N_2}}{\tau_2} \tag{7}$$

To normalize Eqs. (6) and (7);.

Referring to Eq. (6), assuming $N_1 = Q_w[\overline{N_2}(\mho_1) - 1]$, therefore $\overline{N_2} = \frac{Q_w + N_1}{Q_w \mho_1}$ and $\frac{d\overline{N_2}}{dt} = \frac{dN_1}{Q_w \mho_1 dt}$. Also, dividing the whole Eq. (6) by q_1 in order to cancel out q_1 and then substituting I_p for $\frac{L_p}{q_1}$ and then multiplying the entire Eq. (6) by τ_2 where $\vartheta = \frac{t}{\tau_2}$ gives:

$$\frac{dI_p}{dt} = \frac{\tau_2}{Q_w \mho_1} (Q_w + N_1) + 2LQ_0 I_p N_1 \frac{\tau_2}{t_R} - 2L\alpha_{th} I_p \frac{\tau_2}{t_R} \tag{8}$$

Likewise, referring to Eq. (7), assuming $N_2 = Q_w[\overline{N_2}(\mho_2) - 1]$, therefore $\overline{N_2} = \frac{Q_w + N_2}{Q_w \mho_2}$ and $\frac{d\overline{N_2}}{dt} = \frac{dN_2}{Q_w \mho_2 dt}$. Also, dividing the whole Eq. (7) by q_1 where $I_p = \frac{L_p}{q_1}$ and then multiplying the entire Eq. (7) by τ_2 where $\vartheta = \frac{t}{\tau_2}$ gives:

$$\frac{\frac{dN_2}{dt} = \frac{PP \tau_2 Q_w \mho_2 q_2}{q_1} [1 - e^{[-q_3(1 - \frac{Q_w + N_2}{Q_w \mho_2})]}] - (\Theta_{12} Q_w \tau_2 \mho_2)}{\pi r_0^2 I_p N_2 - \frac{Q_w + N_2}{q_1}}$$

To eliminate the denominator q_1, we multiply the whole equation above by q_1 to get:

$$\frac{dN_2}{dt} = PP\tau_2 Q_w \mho_2 q_2[1 - e^{[-q_3(1-\frac{Q_w+N_2}{Q_w \mho_2})]}] - (\Theta_{12} Q_w \tau_2 \mho_2) \over \pi r_0^2 I_p N_2 q_1 - (Q_w + N_2) \tag{9}$$

Since $\frac{Q_w+N_1}{Q_w \mho_1} = \frac{Q_w+N_2}{Q_w \mho_2}$; then $N_1 = \frac{N_2 \mho_1 + (\mho_1 - \mho_2) Q_w}{\mho_2}$.

Hence Eq. (8) can be written as:

$$\frac{dI_p}{dt} = \frac{\tau_2}{Q_w \mho_1}(Q_w + \frac{\mho_1 N_2}{\mho_2}) + 2LQ_0(\frac{\tau_2}{t_R})(\frac{\mho_1}{\mho_2}) I_p N_2 - 2L(\frac{\tau_2}{t_R})(\alpha_{th} - (\mho_1 + \mho_2) \over \mho_2 Q_w) I_p \tag{10}$$

Introducing constants, Eq. (10) can be written as:

$$\frac{dI_p}{dt} = K_1(Q_w \frac{\mho_2}{\mho_1} + N_2) + K_2 I_p N_2 - K_3 I_p \tag{11}$$

Where K_1, K_2 and K_3 are:

$$K_1 = \frac{\tau_2}{Q_w \mho_1}$$

$$K_2 = \quad 2LQ_0(\frac{\tau_2}{t_R})(\frac{\mho_1}{\mho_2})$$

$$K_3 = \quad \frac{2L(\frac{\tau_2}{t_R})(\alpha_{th} - (\mho_1 + \mho_2)}{\mho_2 Q_w)}$$

Introducing constants, Eq. (9) can be written as:

$$\frac{dN_2}{dt} = R_1[1 - e^{[-LQ_p(1-\frac{Q_w+N_2}{Q_w \mho_2})]}] - R_2 I_p N_2 - (Q_w + N_2) \tag{12}$$

where R_1 and R_2 re:

$R_1 = PP\tau_2 Q_w \mho_2 q_2$; re-introducing the value of q_2, R_1 becomes:

$R_1 = PP\ \frac{\tau_2 Q_w \mho_2}{\pi r_0^2 L N_0}$ where PP is the pump power at the entrance of the optical fiber.

$R_2 = \frac{(\Theta_{12} Q_w \tau_2 \mho_2)}{\pi r_0^2 q_1}$; re-introducing the value of q_1, R_2 becomes:

$$R_2 = \frac{(\Theta_{12} Q_w \tau_2 \mho_2)}{\pi r_0^2 \frac{Q_o \lambda_g^2 L}{\tau_2 t_R \Theta_{12}} \frac{r_0^2 10^{-3}}{4(\pi r_f)^2}}$$

Eq. (11) is the normalized laser power density and Eq. (12) is the normalized population inversion at meta-stable or upper level 2 of the EDFL. In the simulation, the pump power is a chirp signal, in order to deliver a continuous range of MFs. Therefore, the pump power at the entrance of the fiber becomes:

$$PP(t) = PP_1^0[1 + A_m \sin(2\pi(F_m + cc.t)t] \tag{13}$$

where cc is the chirp coefficient in Hz/s.

Other initial conditions such as the normalized inlet pump power in inverse seconds and the MA (fixed value) are also inputted before running the simulation. The value of the input pump power determines the RF of the laser system. The initial and final MFs and the chirp duration of the modulation are specified in the code such that the chirp may be ascending or descending in frequency. For each run, the simulation uses a random starting point as it is typical in laser transient computations. Due to this, the laser response may not be similar for a particular frequency during up-chirp (ascending MF) and down-chirp (descending MF) since the initial condition is not the same [23]. The simulation code generates the laser response by solving the differential equations using ODE45 (Runge-Kutta 4th order method with adaptive step size). For each input chirp signal, the amplitude of maximum power, at each MF is saved in a file and plotted to generate bifurcation, time domain and frequency domain diagrams which show the behavior of the EDFL.

4. Numerical simulation, analysis and results

Numerical simulations to obtain the bifurcation, time domain and frequency domain diagrams that describe the dynamics of our EDFLL and EDFRL respectively under pump modulation has been carried out using Eqs. (11) and (12). As mentioned earlier, experimental analysis on the same linear and ring laser set-ups has been carried out and reported in our previous publications [25–27]. Results of the numerical simulations show comparable trends to that of the experimental results, specifically in the RFs. The numerical results even seem to give better predictions compared to the experiments for some RFs. The dynamics of the EDFLL and EDFRL is linked to the main RF of the laser which is seen nearby the relaxation oscillation frequency of the laser [12].

4.1. Numerical simulation of the EDFLL under pump modulation

Numerical simulation of the pump modulated EDFLL has been carried out several times with different input conditions; however only three results would be presented here. From our previous publication, the diagram in Fig. 3(a) is the experimental bifurcation diagram obtained by manually tuning the MF from 1 kHz to 60 kHz using a manual function generator [27]. Before modulation, the voltage of the laser (modulation amplitude MA) was fixed at 0.2 V and the laser was pumped at 95 mW power from the laser pump to the EDF which is equivalent to a fixed RF of 7 kHz. During pump modulation, the peak to peak amplitude of the optical output was measured for every frequency change which is plotted as the bifurcation diagram. The dynamic behavior observed has already been explained in details in [27] and can be referred to, however it is important to note that period-doubling bifurcation, regions of optical bi-stability (OB) and chaos were identified. For the numerical simulation, parameters that are close to the experimental ones were used to obtain the normalized parameter values in Table 1. The initial simulation conditions before modulation are: normalized input pump power of 427 s^{-1}, which is equivalent to 95 mW, to give 7 kHz RF; m = 0.25 which is equivalent to 0.2 V; initial and final MF (1 kHz and 60 kHz) and the final end time of the chirp (3 s). These initial conditions enable us obtain an ascending chirp, while for the descending chirp, the initial and final MF are reversed. With the maximum peak intensities obtained from the ascending and descending chirp, the numerical bifurcation diagram in Fig. 3(b) was plotted.

Comparison of the bifurcation diagrams showed that all experimental peaks and branches appear in the numerical bifurcation figure too, except that in some cases there is a slight shift either forward or backward to the next one, two or three frequencies and the heights of the peaks may not be the same in both bifurcation diagrams which is still acceptable [23]. This is not surprising as the reason for this is that the calculations for the values used for numerical simulation may involve some approximations and we consider the averaged intra-cavity laser power across the EDF length. In the real sense, the variations of power along the active medium should be considered but this is not easy to achieve numerically. Also every single loss due to splicing may not be accounted for numerically. More so, the EDF is very sensitive to vibrations and other external perturbations even as simple as a slight shift or touch of the set-up during the experiments that may cause a minor shift in the expected results. It has also been observed that the regions of chaos and the widths of the different OB regions and its profile shape are also correctly predicted to a reasonable extent. Thus, it can be said that the numerical result is very close to the experimental result and acceptable. Similar results have been obtained by other authors [12,20,22,23]. In the experimental bifurcation diagram in Fig. 3(a), resonance peaks appear at (8, 11, 19 and 49) kHz for the approach from low to high frequency and at (9, 14 and 32) kHz vice versa. In the numerical bifurcation diagram, resonance peaks appear at (8, 12, 21 and 48) kHz for the approach from low to high frequency and at (8, 12 and 26) kHz vice versa. The various frequencies at which resonance peak appears are closely related to the natural frequency of the laser system [23]. The very first peak seen from the approach from low to high frequency symbolizes the main RF of the system. Experimentally and numerically, it is at 8 kHz which is a perfect match even though before modulation it was set at 7 kHz. Likewise, other numerical resonance peaks have a small shift from the experimental resonance peaks too. This result is still very much acceptable based on the already explained reasons. Comparison of the time domains and frequency domains (not shown in this paper) from the experimental and numerical bifurcation diagrams showed good agreement too.

To avoid any discrepancy and strongly prove that the numerical model describes our EDFLL well, another numerical result is presented in Fig. 4 wherein the MA is increased to 0.4 V but the RF remains the same. To generate the experimental bifurcation diagram shown in Fig. 4(a), photons were pumped at 107 mW power from the laser pump to the EDF which is equivalent to a fixed RF of 7 kHz at 0.4 V amplitude. Experimental pump modulation from 1 kHz to 60 kHz resulted in the bifurcation diagram in Fig. 4(a). To obtain the numerical bifurcation diagram, the initial simulation conditions before modulation are: normalized input pump power of 390 s^{-1} which is equivalent to 107 mW to give 7 kHz RF; m = 0.38 which is equivalent to 0.4 V; initial and final MF (1 kHz and 60 kHz) and the final end time of the chirp (3 s). The MF was swept in ascending and descending orders and the maximum peak intensities at each MF and for each sweep were plotted to obtain the numerical bifurcation diagram (Fig. 4(b)). Comparison of the

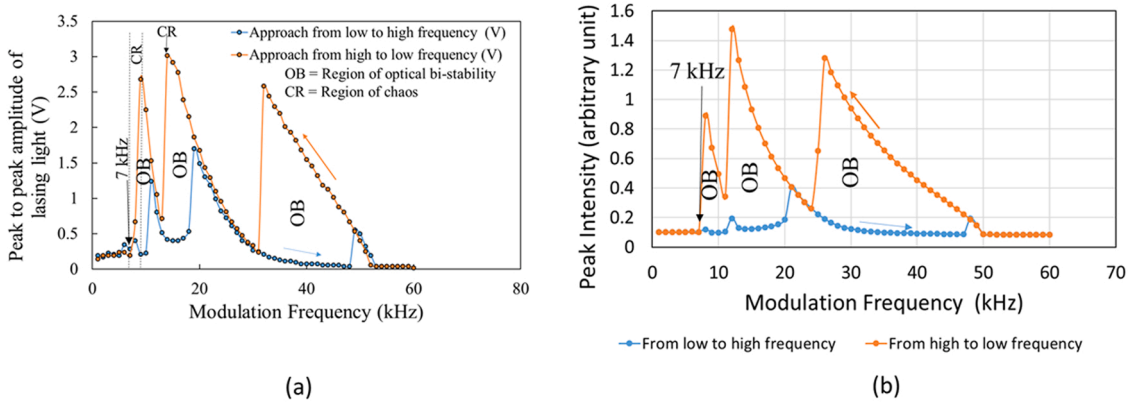

Fig. 3. (a) Experimental [27] and (b) numerical bifurcation diagrams showing the dynamical behaviors of the EDFLL obtained by sweeping the MF from 1 kHz to 60 kHz and vice versa at 0.2 V MA and 7 kHz RF.

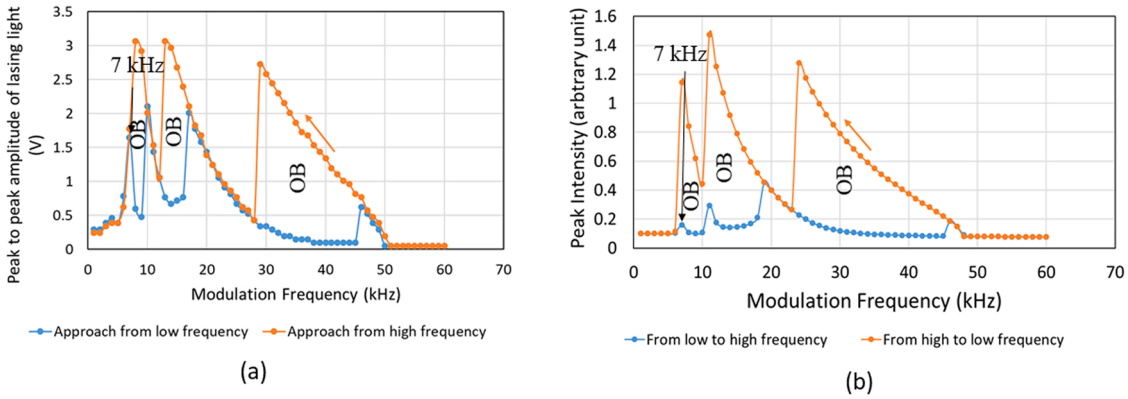

Fig. 4. (a) Experimental and (b) numerical bifurcation diagrams showing the dynamical behaviors of the EDFLL obtained by sweeping the MF from 1 kHz to 60 kHz and vice versa at 0.4 V MA and 7 kHz RF.

experimental and the numerical bifurcation diagrams showed similar characteristics to that of Fig. 3 and good agreement is seen between them. Therefore, the explanation would not be repeated again. In the experimental bifurcation diagram, resonance peaks appear at (7, 10, 17 and 46) kHz for the approach from low to high frequency and at (8, 13 and 22) kHz vice versa. In the numerical bifurcation diagram, resonance peaks appear at (7, 11, 19 and 46) kHz for the approach from low to high frequency and at (7, 11 and 24) kHz vice versa. The very first peak seen from the approach from low to high frequency which is the main RF of the system is at 7 kHz both experimentally and numerically which is a perfect match. Other resonance peaks are also a near match or exactly match each other.

To further support the accuracy of the model for the EDFLL under pump modulation, one more result showing the experimental and numerical bifurcation diagrams is presented in Fig. 5 for input conditions of 0.1 V MA, pump power of 201 mW (equivalent to 13 kHz RF) and MF of 1 kHz to 60 kHz. To obtain the numerical bifurcation diagram, the initial simulation conditions before modulation are: normalized input pump power of 590 s^{-1} which is equivalent to 201 mW to give 13 kHz RF; m = 0.09 which is equivalent to 0.1 V; initial and final MF (1 kHz and 60 kHz) and the final end time of the chirp (3 s). Comparison of the experimental and the numerical bifurcation diagrams showed similar characteristics to that of Figs. 3 and 4 and good agreement is seen between them. In the experimental bifurcation diagram, resonance peaks appear at (16 and 26) kHz for the approach from low to high frequency and at (16 and 21) kHz vice versa. In the numerical bifurcation diagram, resonance peaks appear at (14 and 26) kHz for the approach from low to high frequency and at (14 and 21) kHz vice versa. The main RF of the EDFLL is 13 kHz of which the resonance peaks appear near the RF. The numerical results of the EDFLL are in good agreement with the experimental results.

4.2. *Numerical simulation of the EDFRL under pump modulation*

Several numerical simulations of the pump modulated EDFRL has been carried out with different input conditions but only two results would be presented here. From our previous publication, Figs. 6(a), 7(a), 8(a–c) were obtained from the experimental pump modulation of the EDFRL by manually varying the MF from 1 kHz to 30 kHz using a manual function generator at RFs of (2, 3, 5, 7 and

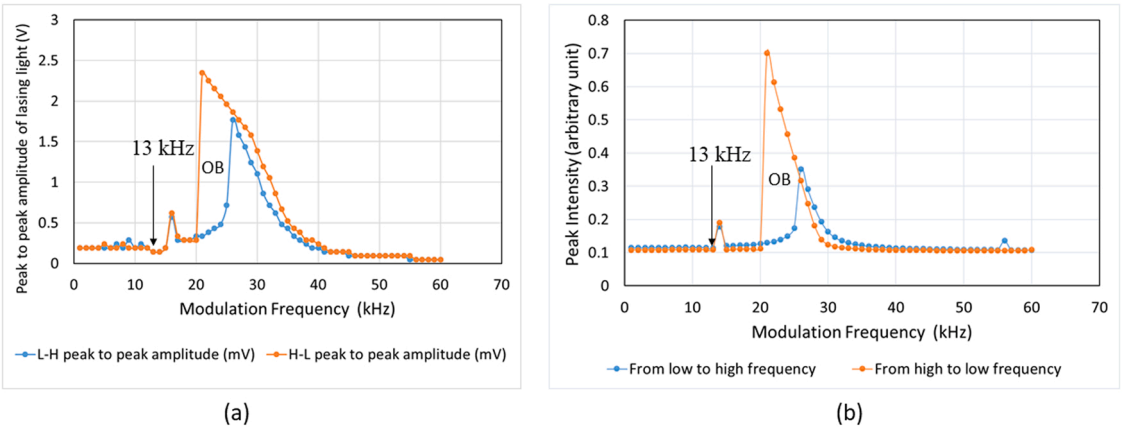

Fig. 5. (a) Experimental and (b) numerical bifurcation diagrams showing the dynamical behaviors of the EDFLL obtained by sweeping the MF from 1 kHz to 60 kHz and vice versa at 0.1 V MA and 13 kHz RF.

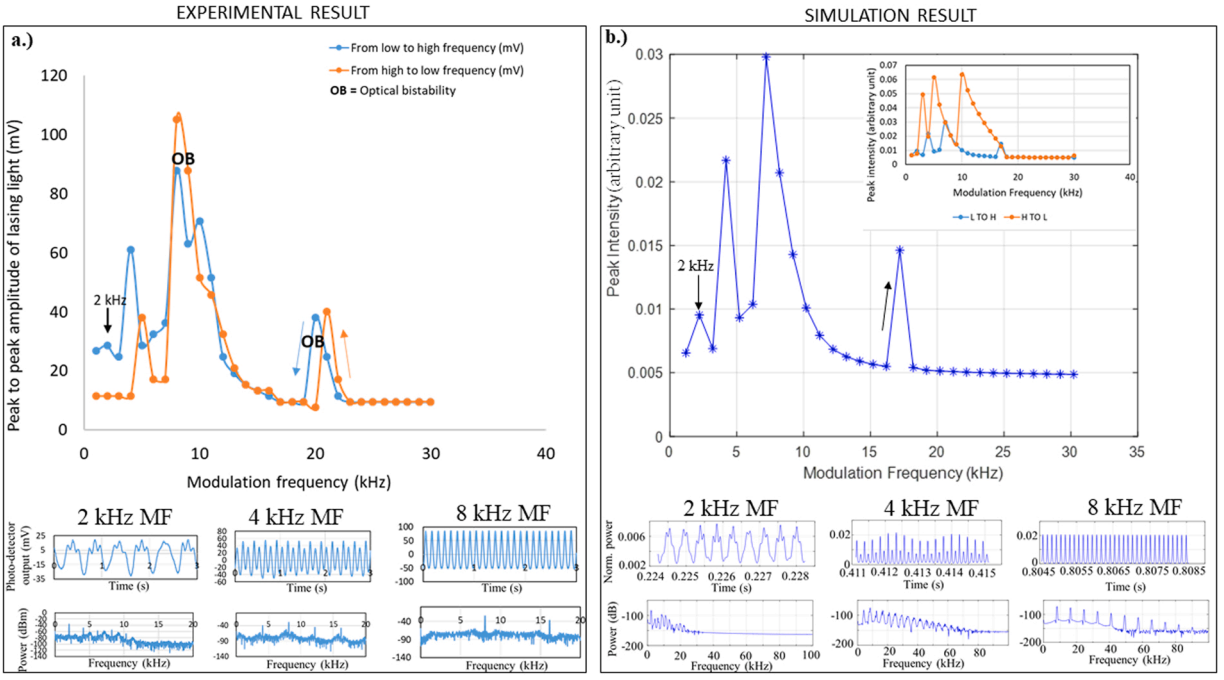

Fig. 6. (a) Experimental and (b) numerical bifurcation diagrams showing the dynamical behaviors of the EDFRL obtained by sweeping the MF from 1 kHz to 30 kHz and vice versa at 0.4 V MA and 2 kHz RF.

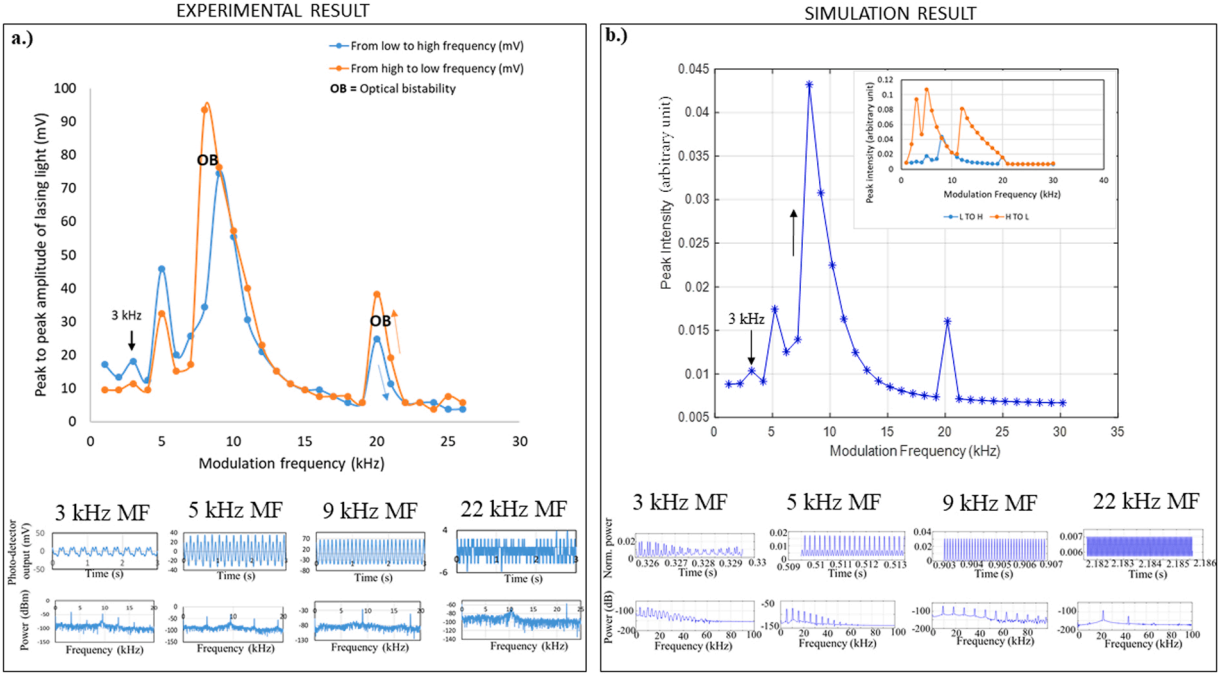

Fig. 7. (a) Experimental and (b) numerical bifurcation diagrams showing the dynamical behaviors of the EDFRL obtained by sweeping the MF from 1 kHz to 30 kHz and vice versa at 0.4 V MA and 3 kHz RF.

10) kHz respectively [25]. These results are grouped as one (group 1) to explain the numerical simulation results; while for comparison and more complacent explanation, the second result presented is of the experimental and numerical simulation of the pump modulated EDFRL from 1 to 60 kHz MF at a RF of 9 kHz and 0.4 V MA which has never been published before.

Based on the relationship established between pump power and resonance frequency, it was concluded in Onubogu et al. [25] that

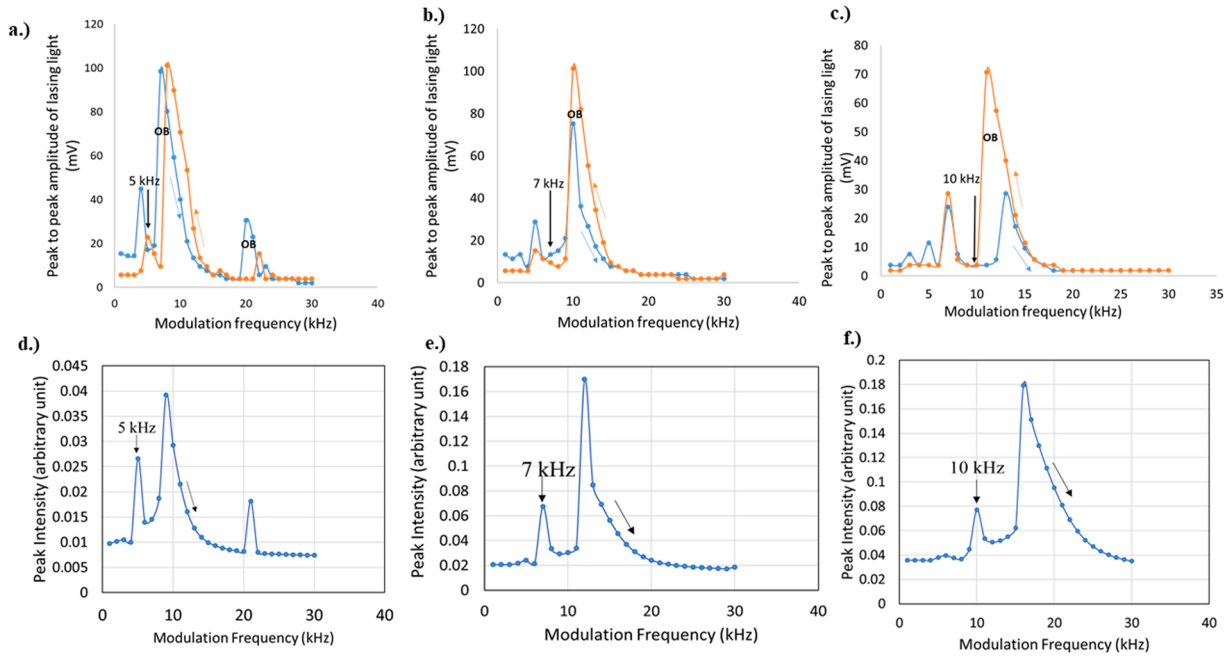

Fig. 8. Experimental [(a), (b), (c)] and numerical [(d), (e), (f)] bifurcation diagrams showing the dynamical behaviors of the EDFRL obtained by sweeping the MF from 1 kHz to 30 kHz and vice versa at 0.4 V MA and 5 kHz RF (a) and (d); 7 kHz RF (b) and (e) and 10 kHz RF (c) and (f).

by adjusting the pump power of the EDFRL from 110.4 mA to 180.7 mW, the RF can be shifted from 2 kHz to 10 kHz frequency range. This short range can be said to be as a result of the long cavity length of the EDRFL and the limitation of the laser pump diode to 245 mW power only. Starting with the first group of results (group 1); before experimental pump modulation, the amplitude of the EDFRL was set to 0.4 V at all times and for the five different experimental results presented (Figs. 6(a), 7(a), 8(a–c)), the laser was pumped at 110.4 mW, 120 mW, 127.6 mW, 150.6 mW and 180.7 mW powers respectively to the EDF which is equivalent to fixed RFs of 2 kHz, 3 kHz, 5 kHz, 7 kHz and 10 kHz respectively. Details of this experimentally pump modulated EDFRL with the exact input conditions as described can be found in our previous publication [25], so this section of this paper would focus more on the numerical results obtained with our model in comparison with the experimental results. During pump modulation, the peak to peak amplitude of the optical output were measured for every MF change both in ascending and descending orders, which are plotted as the bifurcation diagrams. Detailed explanation of the dynamic behaviors observed has already been explained in Onubogu et al. [25] and can be referred to, however it is important to note here that behaviors such as regions of optical bi-stability (OB), period-doubling routes to chaos, and chaos were observed. For the numerical simulation, parameters that are close to the experimental ones were used to obtain the normalized parameter values in Table 1. The initial simulation conditions are presented in Table 2. The initial and final MF were set as 1 kHz and 30 kHz and the final end time of the chirp was set at 3 s

These initial conditions enable us obtain an ascending chirp, while for the descending chirp, the initial and final MF are reversed. With the maximum peak intensities obtained from the ascending and descending chirp, the numerical bifurcation diagrams in Figs. 6 (b), 7(b), 8(d–f) were plotted.

It can be observed that in the bifurcation diagrams of the EDFRL in group 1, the bifurcation diagram was only plotted for ascending chirp i.e. from low MF to high MF. This is because it is easier to compare the numerical bifurcation results with the experimental bifurcation results this way as a strange dynamic behavior was observed for the descending chirp. This strange dynamic behavior was noticed for all five input conditions and the reason for this is still unknown and requires further research. A small inset figure inside Figs. 6(b) and 7(b) illustrate the actual numerical bifurcation diagram obtained from plotting the peaks from both ascending and descending chirps. It shows clearly that the laser dynamics obtained from the numerical descending chirp does not match that obtained

Table 2
Initial conditions for numerical pump modulation of EDFRL.

Resonance Frequency, RF (kHz)	Normalized input power (s^{-1})	Experimental input power (mW)	Normalized modulation amplitude, (symbolized as 'm' in simulation)	Modulation amplitude, MA (V)
2	70	110.4	0.38	0.4
3	94	120.0	0.38	0.4
5	104	127.6	0.38	0.4
7	220	150.6	0.38	0.4
10	400	180.7	0.38	0.4

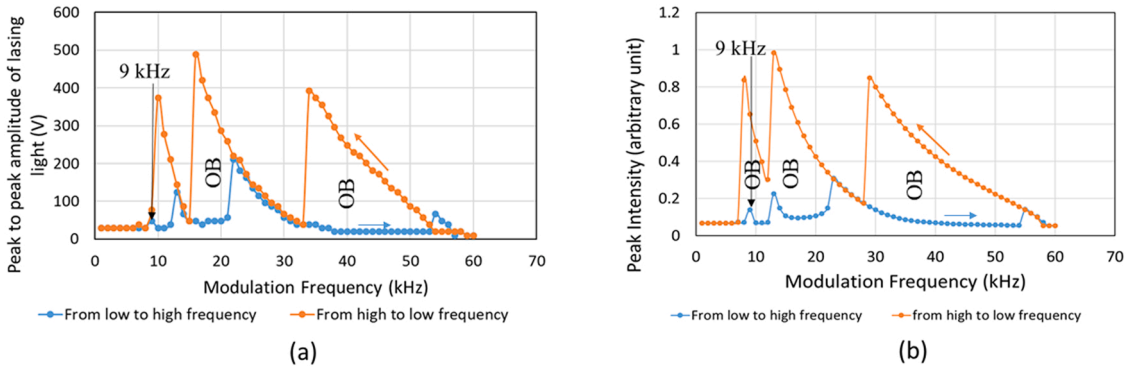

Fig. 9. (a) Experimental and (b) numerical bifurcation diagrams showing the dynamical behaviors of the EDFRL obtained by sweeping the MF from 1 kHz to 60 kHz and vice versa at 0.4 V MA and 9 kHz RF.

from the experimental descending chirp. It is really a new strange occurrence that with the same normalized rate equations, the experimental and numerical bifurcation diagrams obtained from the ascending chirp matches well to a reasonable extent (see Figs. 6–8); whereas the experimental bifurcation diagram obtained from the descending chirp does not match that obtained numerically. Hence, we can confidently say that the bifurcation diagram of the numerical descending chirp for group 1 is correctly predicted because all the other results obtained for other input values of RF and MA (including those not presented in the manuscript) gave similar trends numerically which matched with the experimental result. This entails that the strange behavior is from the experimental result and not the numerical result. We actually presented this result regardless of the strange behavior because it might have an application in the future based on further studies and if so, the model might then be further modified based on the results. To further confirm that the model is correct, another result for the EDFRL under pump modulation (Fig. 9(a) and (b)) is also presented to show that the experimental and numerical results match well. However, it is important to note that during group 1 experiments, there were lots of uncontrolled background noise but we cannot confirm that the background noise is the reason for the strange behavior as it is a known fact that frequency modulation is not really affected by noise unlike in amplitude modulation [30]. Even during the numerical simulation, high amplitude white noise was included during pump modulation and no significant changes were seen in the bifurcation diagrams with and without noise.

Comparison of the experimental and the numerical bifurcation diagrams for group 1 showed similar characteristics to that of Fig. 3 and good agreement is seen between them. In the experimental bifurcation diagram (Fig. 6(a)) when the RF is 2 kHz, resonance peaks appear at (2, 4, 8 and 20) kHz for the approach from low to high frequency and at (5, 8 and 21) kHz vice versa. In the numerical bifurcation diagram (Fig. 6(b)) obtained from ascending chirp only, resonance peaks appear at (2, 4, 7 and 17) kHz. The main RF of the system is 2 kHz of which a peak is seen both experimentally and numerically. This is a perfect match. The time and frequency domains are also shown for some MFs to show the similarities in the pattern both experimentally and numerically. Similarly, in the experimental bifurcation diagram (Fig. 7(a) when the RF is 3 kHz, resonance peaks appear at (3, 5, 9 and 20) kHz for the approach from low to high frequency and at (3, 5, 8 and 20) kHz vice versa. In the numerical bifurcation diagram (Fig. 7(b) obtained from ascending chirp only, resonance peaks appear at (3, 5, 8 and 20) kHz. The main RF of the system is 3 kHz of which a peak is seen both experimentally and numerically. The time and frequency domains are also shown for some MFs to show the similarities in the pattern both experimentally and numerically. Furthermore, in the experimental bifurcation diagram (Fig. 8(a)) when the RF is 5 kHz, resonance peaks appear at (4, 7 and 20) kHz for the approach from low to high frequency and at (5, 8 and 22) kHz vice versa. In the numerical bifurcation diagram (Fig. 8(d)) obtained from ascending chirp only, resonance peaks appear at (5, 9 and 21) kHz. The main RF of the system is 5 kHz of which a peak is seen experimentally at 4 kHz and numerically at 5 kHz which is still acceptable. More so, in the experimental bifurcation diagram (Fig. 8(b)) when the RF is 7 kHz, resonance peaks appear at (5 and 10) kHz for the approach from low to high frequency and at (5 and 10) kHz vice versa. In the numerical bifurcation diagram (Fig. 8(e)) obtained from ascending chirp only, resonance peaks appear at (7 and 12) kHz. The main RF of the system is 5 kHz of which a peak is seen numerically at 5 kHz, however experimentally it is seen at 7 kHz for reasons previously explained. This means the numerical simulation is capable of giving more accurate results. Finally, in the experimental bifurcation diagram (Fig. 8(c)) when the RF is 10 kHz, resonance peaks appear at (3, 5, 7 and 13) kHz for the approach from low to high frequency and at (7 and 11) kHz vice versa. In the numerical bifurcation diagram (Fig. 8(f)) obtained from ascending chirp only, resonance peaks appear at (10 and 16) kHz. The main RF of the system is at 10 kHz of which a peak is seen numerically at 10 kHz, however experimentally it is seen at 7 kHz for reasons previously explained. This confirms again that the numerical simulation is capable of giving more accurate results especially at higher RFs. Other resonance peaks for all the numerical and experimental bifurcation diagrams are also a near match or exactly match each other. Thus, the numerical results are in good agreement with the experimental results.

Regardless of this strange behavior observed for the descending chirp, it can still be concluded that our model describes the EDFRL well and also shows that even in the presence of a lot of background noise, the EDFRL shows the same behavior as in the absence of noise. This makes the EDFRL a very good sensor in areas where there a lots of background noise such as water, oil or gas pipelines, as it is still sensitive at low frequencies regardless of the noise. It can be used to detect leakage and the leak locations in these pipelines. It is of importance to note this feature because it has been observed that some authors only show the laser dynamics/bifurcation diagram of

their laser starting from around 8 kHz MF because below 7 kHz MF they notice an amplitude-modulation-like lasing waveform [20]. In our case, it is different. In our previous publication, we elaborated on this experimentally [25].

To avoid any discrepancy based on group 1 results and to strongly prove that our numerical model describes our EDFRL well, we present another numerical result in Fig. 9. It is vital to note that further experimental and theoretical analysis were carried out using various RFs and MAs (not presented in this paper) of which the results obtained are similar to that of Fig. 9 as expected. This means the accuracy of the model can be guaranteed. To generate the experimental bifurcation diagram (which was performed on a different day from group 1 experiments and in a quiet environment), the EDFRL was pumped at 188.6 mW power which is equivalent to a fixed RF of 9 kHz at 0.4 V MA. Experimental pump modulation from 1–60 kHz resulted in the bifurcation diagram in Fig. 9(a). To obtain the numerical bifurcation diagram, the initial simulation conditions before modulation are: normalized input pump power of 390 s^{-1} which is equivalent to 188.6 mW to give 9 kHz RF; m = 0.38 which is equivalent to 0.4 V; initial and final MF (1 kHz and 60 kHz) and the final end time of the chirp (3 s). The MF was swept in ascending and descending orders and the maximum peak intensities at each MF and for each sweep were plotted to obtain the numerical bifurcation diagram (Fig. 9(b)). Comparison of the experimental and the numerical bifurcation diagrams showed similar characteristics to that of Fig. 3 and good agreement is seen between them. In the experimental bifurcation diagram, resonance peaks appear at (9, 13, 21 and 54) kHz for the approach from low to high frequency and at (10, 16 and 34) kHz vice versa. In the numerical bifurcation diagram, resonance peaks appear at (9, 13, 23 and 55) kHz for the approach from low to high frequency and at (8, 13 and 22) kHz vice versa. The very first peak seen from the approach from low to high frequency, which is the main RF of the system is at 9 kHz both experimentally and numerically which is a perfect match. Other resonance peaks are also a near match or exactly match each other. The numerical results are in good agreement with the experimental results.

5. Conclusion

The dynamics of pump-modulated EDFLL and EDFRL has been numerically investigated in comparison with the dynamics of experimentally pump-modulated EDFLL and EDFRL. Parameters similar to the experimental conditions were used in the numerical simulations. The bifurcation diagrams showing the behavior of the EDFLL and EDFRL both experimentally and numerically have been presented and comparisons made in details. It has been observed that period-doubling bifurcation, regions of optical bi-stability (OB) and chaos were identified in both results for EDFLL and EDFRL and also the regions of chaos and the widths of the different OB regions and its profile shape are also correctly predicted to a reasonable extent. A new strange dynamic behavior which requires further studies was observed based on the numerical results for the descending chirp of the EDRFL under certain pump modulation conditions. Regardless of this strange behavior observed for the descending chirp, it can still be concluded that our model describes the EDFRL well and also shows a high propensity of the EDFRL to be used as a very good sensor in areas where there are lots of background noise such as water, oil or gas pipelines to detect leakage, as it is sensitive even at low frequencies irrespective of the noise. In conclusion, our modified laser model has been shown to describe our experimental results well and new experimental results presented confirm the validity and accuracy of the improved numerical model.

Funding

This work was supported by TRGS, Ministry of Education Malaysia (TRGS, MOE) [TRGS/1/2016/UTAR/01/2/1]; UTARRF, UTAR [IPSR/RMC/UTARRF/2019-C1/P01].

Declaration of Competing Interest

The authors declare that they have no known competing financial interests or personal relationships that could have appeared to influence the work reported in this paper.

References

[1] S. Diaz, D. Leandro, M. Lopez-Amo, Stable multiwavelength erbium fiber ring laser with optical feedback for remote sensing, J. Lightwave Technol. 33 (12) (2015) 2439–2444, https://doi.org/10.1109/jlt.2014.2365257.
[2] L.G. Luo, P.L. Chu, H.F. Liu, 1 GHz optical communication system using chaos in erbium-doped fiber lasers, IEEE Photon. Technol. Lett. 12 (2000) 269–271.
[3] L.G. Luo, P.L. Chu, Optical secure communications with chaotic erbium-doped fiber lasers, J. Opt. Soc. Am. B 15 (1998) 2524–2530.
[4] G.D. VanWiggeren, R. Roy, Optical communication with chaotic waveforms, Phys. Rev. Lett. 81 (1998) 3547–3550.
[5] G.D. VanWiggeren, R. Roy, Communication with chaotic lasers, Science 279 (1998) 1198–1200.
[6] H. Arellano-Sotelo, A.V. Kir'yanov, Y.O. Barmenkov, V. Aboites, The use of nonlinear dynamics of erbium-doped fiber laser at pump modulation for intra-cavity sensing, Opt. Laser Technol. 43 (2011) 132–137, https://doi.org/10.1016/j.optlastec.2010.05.017.
[7] M.J.F. Digonnet, Rare earth doped fiber lasers and amplifiers. Revised and Expanded, second ed., Marcel Dekker, New York, 2001.
[8] C.H. Pua, S.F. Norizan, S.W. Harun, H. Ahmad, Non-membrane optical microphone based on longitudinal modes competition, Sens. Actuators A Phys 168 (2) (2011) 281–285, https://doi.org/10.1016/j.sna.2011.04.034.
[9] C.H. Pua, W.Y. Chong, H. Ahmad, Instantaneous response of wide area intrusion sensor with long haul monitoring capability, IEEE Photonics Technol. Lett. 25 (23) (2013) 2255–2258, https://doi.org/10.1109/LPT.2013.2284608.
[10] S.L. Woon, K.M. Kwan, W.Y. Chong, H.S. Lin, C.H. Pua, Cascaded acoustic wave sensors based on erbium-doped fibre laser dynamics for intrusion zone identification, IEEE Sensors 17 (6) (2017) 1893–1898, https://doi.org/10.1109/JSEN.2017.2655019.
[11] U. Sharma, C.S. Kim, J.U. Kang, Highly stable tunable dual-wavelength Q-switched fibre laser for DIAL applications, IEEE Photonics Technol. Lett. 16 (2004) 1277–1279.

[12] A.N. Pisarchik, A.V. Kir'yanov, Y.O. Barmenkov, Dynamics of an erbium-doped fiber laser with pump modulation: theory and experiment, J. Opt. Soc. Am. B 22 (10) (2005) 2107–2114, https://doi.org/10.1364/JOSAB.22.002107.
[13] A.N. Pisarchik, Y.O. Barmenkov, A.V. Kir'yanov, Experimental characterization of the bifurcation structure in an erbium-doped fiber laser with pump modulation, IEEE J. Quantum Electron. 39 (12) (2003) 1567–1571.
[14] R.J. Reategui, A.V. Kir'yanov, A.N. Pisarchik, Y.O. Barmenkov, N.N. Il'ichev, Experimental study and modelling of coexisting attractors and bifurcations in an erbium-doped fiber laser with diode-pump modulation, Laser Phys. 14 (9) (2004) 1–5.
[15] A.N. Pisarchik, Y.O. Barmenkov, Locking of self-oscillation frequency by pump modulation in an erbium-doped fiber laser, Opt. Commun. 254 (2005) 128–137, https://doi.org/10.1016/j.optcom.2005.05.028.
[16] A.N. Pisarchik, Y.O. Barmenkov, A.V. Kir'yanov, Experimental demonstration of attractor annihilation in a multi-stable fiber laser, Phys. Rev. E 68 (2003), 066211.
[17] E. Lacot, F. Stoeckel, M. Chenevier, Dynamics of an erbium doped fiber laser, Phys. Rev. A 49 (1994) 3997–4008, https://doi.org/10.1364/JOSAB.22.002107.
[18] E. Lacot, F. Stoeckel, M. Chenevier, Spectral and temporal behavior of an erbium doped fiber laser, J. de Physique IV Proceedings, EDP Sciences, 1991, 01 (C7), 357–362. doi: 10.1051/jp4:1991794. jpa-00251037.
[19] L. Luo, T.J. Tee, P.L. Chu, Bistability of erbium-doped fiber laser, Opt. Commun. 146 (1998) 151–157, https://doi.org/10.1016/S0030-4018(97)00502-6.
[20] L. Luo, T.J. Tee, P.L. Chu, Chaotic behaviour in erbium-doped fiber-ring lasers, J. Opt. Soc. Am. B 15 (3) (1998) 972–978, https://doi.org/10.1364/JOSAB.15.000972.
[21] T.S. Kruger, P.C. Rech, Dynamics of an erbium-doped fiber dual-ring laser, Eur. Phys. J. D At. Mol. Opt. Phys. 66 (12) (2012) 3997–4008, https://doi.org/10.1140/epjd/e2011-20396-4.
[22] G. Kumar, R. Vijaya, Dynamical features of loss and pump modulation in an erbium-doped fiber ring laser, J. Opt. 17 (125402) (2015) 1–9, https://doi.org/10.1088/2040-8978/17/12/125402.
[23] I.J. Sola, J.C. Martin, J.M. Alvarez, Non-linear response of a unidirectional erbium-doped fiber ring laser to a sinusoidally modulated pump power, Opt. Commun. 212 (2002) 359–369.
[24] I.J. Sola, J.C. Martin, J.M. Alvarez, Analytical treatment for the study of an erbium-doped fiber ring laser fed by a sinusoidally modulated pump power, Opt. Commun. 258 (2006) 59–66.
[25] N.O. Onubogu, C.H. Pua, H.S. Lin, A. Faidz, The dynamic behavior of non-polarized erbium-doped fiber ring laser under experimental pump modulation, Optik 207 (2020), 164442.
[26] N.O. Onubogu, C.H. Pua, Dynamic behavior of a pump-modulated erbium-doped fiber linear laser with single fiber Bragg grating, in: A. Sivasubramanian, P. N. Shastry, P.C. Hong (Eds.), Futuristic Communication and Network Technologies, Lecture Notes in Electrical Engineering, 792, Springer, Singapore, 2022, https://doi.org/10.1007/978-981-16-4625-6_28.
[27] N.O. Onubogu, C.H. Pua, H.S. Lin , A. Faidz, Dynamics of a highly sensitive erbium-doped Fabry-Perot fiber (EDFBF) laser sensor under pump modulation, in: Proceedings of the Twenty Fourth Microoptics Conference (MOC), 2019, 262–263, ⟨https://doi.org/10.23919/MOC46630.2019.8982878⟩.
[28] C.H. Pua, H. Ahmad, S. Harun, R. De La Rue, Direct airborne acoustic wave modulation of Fabry–Perot fiber laser (FPFL) over 100 kHz of operating bandwidth, Appl. Opt. 51 (15) (2012) 2772–2777, https://doi.org/10.1364/AO.51.002772.
[29] Jaimes Reátegui , 2004, Dynamic of complex system with parametric modulation: Duffing oscillators and a fiber laser, Tesis de Doctorado en Ciencias (Óptica), Centro de Investigaciones en Óptica, A.C. León, Guanajuato, 133.
[30] M.G. Crosby, Frequency modulation noise characteristics, in Proceedings of the institute of Radio Engineers, 25 (4), 1937, 472–514, doi: 10.1109/JRPROC.1937.229050.